Available online at www.sciencedirect.com
ScienceDirect
Journal of Power Sources 166 (2007) 478–484
JOURNAL OF POWER SOURCES
www.elsevier.com/locate/jpowsour

Characterization of electrolytic Co_3O_4 thin films as anodes for lithium-ion batteries

Han-Chang Liu, Shiow-Kang Yen *

Department of Material Engineering, National Chung Hsing University, Taichung 40227, Taiwan

Received 16 August 2006; received in revised form 25 January 2007; accepted 30 January 2007
Available online 4 February 2007

Abstract

The electrolytic deposition of Co_3O_4 thin films on stainless steel was conducted in $Co(NO_3)_2$ aqueous solution for anodes in lithium-ion thin film batteries. Three major electrochemical reactions during the deposition were discussed. The coated specimens and the coating films carried out at −1.0 V (saturated KCl Ag/AgCl) were subjected to annealing treatments and further characterized by XRD, TGA/DTA, FE-SEM, Raman spectroscopy, cyclic voltammetry (CV) and discharge/charge cyclic tests. The as-coated film was β-$Co(OH)_2$, condensed into CoO and subsequently oxidized into nano-sized Co_3O_4 particles. The nano-sized Co_3O_4, CoO, Li_2O and Co particles revealed their own characteristics different from micro-sized ones, such as more interfacial effects on chemical bonding and crystallinity. The initial maximum capacity of Co_3O_4 coated specimen was 1930 mAh g^{-1} which much more than its theoretical value 890 mAh g^{-1}, since the nano-sized particles offered more interfacial bondings for extra sites of Li^+ insertion. However, a large ratio of them was trapped, resulting in a great part of irreversible capacity during the first charging. Still, it revealed a capacity 500 mAh g^{-1} after 50 discharged-charged cycles.

Keywords: Electrolytic deposition; Nano-sized Co_3O_4; Thin film; Raman spectroscopy

1. Introduction

Rechargeable solid-state batteries have long been considered an attractive power source for a wide variety of applications, and in particular, lithium-ion batteries are emerging as the technology of choice for portable electronics. One of the main challenges in the design of these batteries is to ensure that the electrodes maintain their integrity during hundreds of discharge-recharge cycles.

Recently, tin-based oxides have been intensively investigated [1–3]. Courtney and Dahn reported that the high specific capacity of tin-based oxides was due to the formation of Li_2O and Sn-Li alloys. However, the large volume change induced during the charge-discharge process caused internal degradation, resulting in the loss of capacity with a poor cycle life. The microstructure of metal oxide or alloy anodes is believed to have an important role on the cycle life performance.

Poizot have already proposed a class of new anode materials which are composed of nano-sized transition-metal oxides, such as nickel oxides, cobalt oxides and iron oxides for lithium-ion batteries [4]. Among them, cobalt oxides demonstrated the best electrochemical properties as lithium storage materials in Li-ion cells. Badway et al. [5] studied in the form of Li/CoO (Co_3O_4) half-cells whose reversible capacity achieved in the 750–1000 mAh g^{-1} range. Wang et al. [6] demonstrated CoO electrode with a stable reversible lithium storage capacity about 300 mAh g^{-1} after 30 cycles. Larcher et al. [7] clearly indicated that several factors govern the reduction path for cobalt oxide. In the first stage of the reduction, small Co_3O_4 domains, or lower intermittent applied discharge currents preferentially led to CoO, whereas large domains as well as fast discharge rates favored the formation of inserted $Li_xCo_3O_4$. Slight changes in temperature were found to affect the overall reaction as well. Li et al. [8] also demonstrated that the electrode properties of Co_3O_4 nanotubes are much better than that of Co_3O_4 nanorods or nanoparticles owing to their hollow and nanostructure characters.

The technologies manufacture thin film cobalt oxides by various methods such as electron-beam evaporation [9], electrochemical depositions [10], chemical vapor deposition [11],

* Corresponding author. Tel.: +886 4 22852953; fax: +886 4 22857017.
E-mail address: skyen@dragon.nchu.edu.tw (S.-K. Yen).

0378-7753/$ – see front matter © 2007 Elsevier B.V. All rights reserved.
doi:10.1016/j.jpowsour.2007.01.072

sol–gel [12], and pulsed laser deposition [13] have been reported. Among these methods of deposition, electrochemical techniques are employed frequently because very thin and uniform films with a high degree of adherence and coatings on substrates of complex shape can be prepared.

In this study, the cathodic deposition of cobalt oxides Co_3O_4 as the activated materials for lithium-ion battery is discussed. The coated specimen powders and the coating films were characterized by XRD, TGA/DTA, FE-SEM, Raman spectroscopy, cyclic voltammetry (CV) and discharge/charge cyclic tests.

2. Experimental

2.1. Substrate preparation

304 stainless steel (S.S.) and platinum sheet (Pt) substrates were cut into 1 cm × 1 cm plates which cleaned in deionized water and acetone by ultrasonic cleaner then dried at room temperature.

2.2. Cathodic polarization tests and depositions

To investigate the electrochemical reactions in $Co(NO_3)_2$ aqueous solution variation nearby the cathode electrode at various voltages, the platinum plates were electrochemically polarized in the 0.01 M $Co(NO_3)_2$ aqueous solution, which was assigned to solution A, by using an EG&G VersaStat **II** Potentiostat and M 352 software. To investigate the effects of O_2 and H^+ concentrations on the cathodic reaction, the polarization tests were also conducted in HCl added and deaerated by N_2 purging, assigned to solutions B and C, respectively. The potential range was swept from the equilibrium potential of the platinum to a final potential of −2.5 V (versus the potential of saturated KCl, Ag/AgCl), with a scanning rate of 0.167 mV s^{-1}. According to the above results, the deposition was carried out in solution A at −1 V (versus the potential of saturated KCl, Ag/AgCl) on 304 stainless steel substrates for further characterization and electrochemical performance.

2.3. XRD and FE-SEM

The crystal structures of the as-coated, annealed at 200, 300, 400, 600 and 1000 °C for 5 h, charged and discharged specimens were analyzed by X-ray diffraction (XRD) in a MAC MO3X-HF diffractometer, with Cu Kα radiation (λ = 1.54185 Å), 2θ in the range 10°–70°, at a scanning rate of 1° min^{-1}, a voltage of 40 kV, and a current of 30 mA. The surface morphology of the coated specimens was observed by a field-emission scanning electron microscope (FE-SEM, JEOL JSM-6330TF microscope).

2.4. TG-DTA

In order to investigate the thermal effects on coatings, the as-deposited films on Pt were scraped for thermal gravitational/differential thermal analysis (TG/DTA). Prior to tests, the powders were dried at room temperature for 24 h and then carried out at a heating rate of 5° min^{-1} under static air between 20 and 1000 °C, using a Seiko TG/DTA SSC 5000 analyzer with the simultaneous recording of weight variations.

2.5. Electrochemical performance

Test cells were fabricated with the cobalt oxide coated stainless steels as the working electrode, and metallic Li as the counter and reference electrodes in argon gas filled glove box. 1.0 M $LiClO_4$ solution in propylene carbonate was used as the electrolyte. The cyclic voltammetric (CV) measurement was carried out between 0.01 and 3.0 V (versus Li/Li^+) at a scanning rate of 0.5 mV s^{-1} on an EG&G model 273 potentiostat/galvanostat. The discharge/charge measurements were performed at a current density of 50 μA (C/2), and showed voltage behaviors over the voltage range 0.01–3.0 V versus Li/Li^+ using a Maccor 2200 apparatus at room temperature.

2.6. Raman measurements

Raman analyses of the as-coated, post-charged and post-discharged specimens were measured ex situ at room temperature using a Raman PL Microspectrometer (Tokyo Instruments, INC) with He-Ne Laser (632.8 nm) as the excitation source and collected range from 400 to 800 cm^{-1}.

3. Results and discussion

3.1. Cathodic reactions

There are three regions divided on the polarization curves, as shown in Fig. 1. The diffusion-limited current densities corresponding to region I and region II for solution A aerated with air, solution B added with HCl, solution C deaerated with N_2 were given in Table 1. According to the components in solution A, several possible reactions are suggested as following:

$$O_2 + 4H^+ + 4e^- \rightarrow 2H_2O \quad E^\circ = 1.032\,\text{V vs.Ag/AgCl} \quad (1)$$

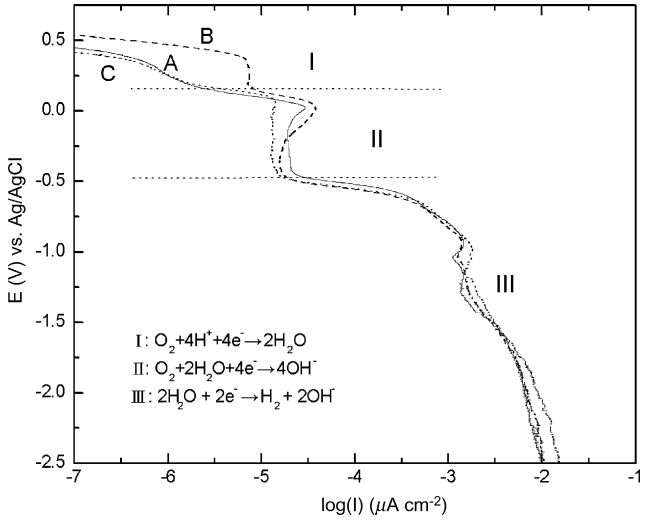

Fig. 1. Cathodic polarization curves of the platinum in 0.01 M $Co(NO_3)_2$ aqueous solutions aerated in air (solid line), added HCl (dash line) and deaerated with N_2 (dot line) was assigned to curves A, B, and C, respectively.

Table 1
The diffusion-limited current densities of polarization curves corresponding to regions I and II in the 0.01 M $Co(NO_3)_2$ aqueous solutions aerated with air, added with HCl and deaerated with N_2 which were assigned to solutions A, B, and C, respectively

Solution	pH	O_2 (mg L^{-1})	Limiting current density (μA cm^{-2})	
			Region I	Region II
A	5.48	7.48	1.73	20.61
B	3.75	7.42	7.30	16.42
C	5.46	0.65	1.73	13.39

$$O_2 + 2H_2O + 4e^- \rightarrow 4OH^- \quad E^\circ = 0.204\,\text{V vs.Ag/AgCl} \tag{2}$$

$$H^+ + e^- \rightarrow H_2 \quad E^\circ = -0.197\,\text{V vs.Ag/AgCl} \tag{3}$$

$$Co^{2+} + 2e^- \rightarrow Co \quad E^\circ = -0.083\,\text{V vs.Ag/AgCl} \tag{4}$$

$$2H_2O + 2e^- \rightarrow H_2 + 2OH^- \quad E^\circ = -1.025\,\text{V vs.Ag/AgCl} \tag{5}$$

3.1.1. Region I (+0.47 to +0.17 V versus saturated Ag/AgCl)

The solution pH value was modified from 5.48 down to 3.75 resulting in the first limiting current density shift apparently from 1.73 to 7.30 μA cm^{-2}, as shown in Fig. 1 curves A and B. However the curve C was not obviously different from curve A, representing no effect of O_2 concentration on the reaction rate. This means that the reaction rate was controlled by the diffusion rate of H^+. Reactions (1) and (3) are both possible. When considering the equilibrium potentials, only reaction (1) is possible.

3.1.2. Region II (+0.17 to −0.46 V versus saturated Ag/AgCl)

The deaerated treatment by N_2 purging revealed the second limiting current density shift from 20.61 down to 13.39 μA cm^{-2} as shown in Fig. 1 curves A and C. Obviously, the reaction rate was controlled by the diffusion rate of O_2. In other words, reaction (2) dominates in region II. The peak current density of curve B increased to 35.08 μA cm^{-2} was resulted from the adding effect of reaction (1).

3.1.3. Region III (−0.46 to −2.50 V versus saturated Ag/AgCl)

At the region all three curves had jiggled seriously below −1.0 V accompanied with a large amount of bubbles poured out from the solutions. The phenomenon was resulted from the reduction H_2O in reaction (5). At the same time, a lot of hydrogen and hydroxyl ions were formed nearby the electrode, favoring the deposition of hydroxide compound. The most optimistic deposition condition was controlled at −1.0 V to obtain the uniform coating films. The XRD of the as-deposited powders exhibited the (1 0 1), (0 0 1), (1 0 0) and (1 0 2) peaks of β-$Co(OH)_2$ according to JCPDS 30-0443, as shown in Fig. 2.

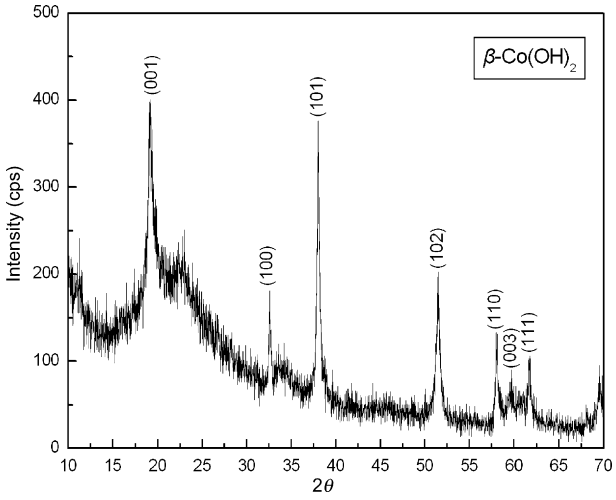

Fig. 2. XRD patterns of the as-deposited powders scraped from the electrode surface.

This means that the deposition of β-$Co(OH)_2$ was resulted from the following chemical reaction:

$$Co^{2+} + 2OH^- \rightarrow Co(OH)_2 \tag{6}$$

3.2. Phase transformations and crystal structures

The TGA curve of cobalt hydroxide powders can be divided into regions A, B, C and D as shown in Fig. 3. Region A from 25 to 170 °C about 5% weight loss was resulted from the evaporation of physically adsorbed water. Region B from 170 to 210 °C, revealed obvious weight loss about 26% and an endothermic reaction (DTA curve). This was resulted from the decomposition of cobalt hydroxide into amorphous cobalt mono-oxide by the removal of chemisorbed water [14–16],

$$Co(OH)_2{\cdot}H_2O \rightarrow CoO + 2H_2O \tag{7}$$

However no CoO peaks were observed in the XRD pattern as shown in Fig. 4 diagrams (b), (c) and (d). Only Co_3O_4 were

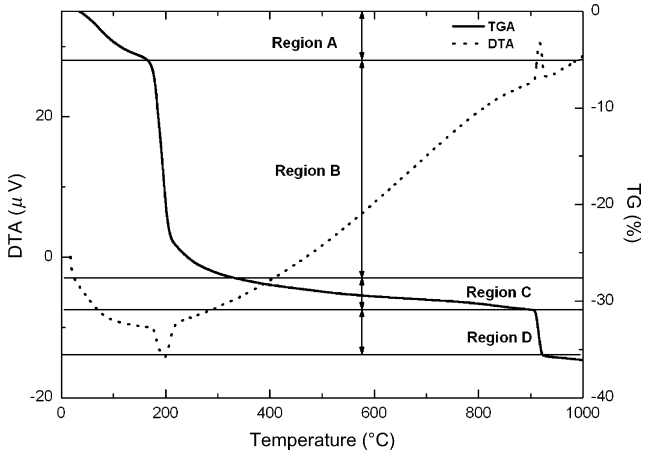

Fig. 3. TG/DTA diagrams of the as-deposited powders heated in air at the increasing temperature rate of 5 °C min^{-1}.

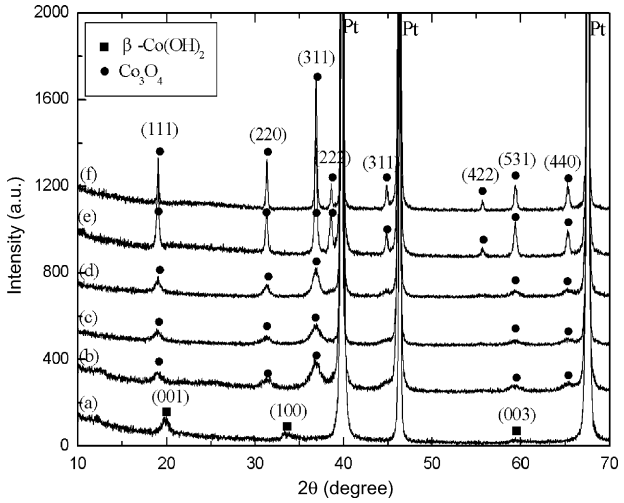

Fig. 4. Ex situ XRD patterns of (a) the as-deposited specimen, annealed at (b) 200 °C, (c) 300 °C, (d) 400 °C, (e) 600 °C, (f) 1000 °C, for 5 h respectively.

found. This means

$$3CoO + 1/2O_2 \rightarrow Co_3O_4 \quad (8)$$

subsequently occurred. In other words, reaction (7) and (8) are linked. The argument of reaction (7) and (8) is supported by the weight ratio of retained 69.11% to weight loss 26% being equal to the molecular weight ratio of Co_3O_4 to $6H_2O - 1/2O_2$ (241:92), as shown in regions B and C. Consistently, the crystallinity of Co_3O_4 structure was increased with increasing annealing temperature, as shown in Fig. 4. About 4.79% weight loss in region D and an exothermic peak found at 915 °C can be ascribed to the thermal decomposition [17],

$$Co_3O_4 \rightleftarrows 3CoO + 1/2O_2 \quad (9)$$

It was also supported by the ratio of weight loss 4.79% to retained weight 64.32% being equal to the weight ratio of $1/2O_2$ to 3CoO (16:225). On the other hand, it has been reported that reaction (9) is reversible [18]. When the temperature was lowered to the room temperature, CoO was transformed into Co_3O_4, as shown in Fig. 4 diagram (f).

3.3. Electrochemical characterization

The first and second cyclic voltammograms (CV) of cobalt oxides measured at a scan rate of 0.5 mV s^{-1} between 0.01 and 3.0 V are shown in Fig. 5. In the first cycle, a large cathodic current peak with a maximum at about 0.85 V and a small one peaked at 0.23 V are observed and three anodic peaks at 1.02, 1.62 and 2.19 V revealed the multi-step extraction process. However, in the second cycle, these two cathodic peaks shift to 0.64 and 1.58 V, respectively. The intensity of the second redox peaks gradually decreases in the subsequent scanning cycles. Earlier report indicated that the plateau of the first discharge and that of the subsequent discharge of Co_3O_4 appeared at 1.18 and 1.2 V, respectively, and those of CoO appeared at 0.8 and 1.5 V, respectively [4]. We note that the second discharge behavior of the Co_3O_4 film electrode fabricated by electrochemical in this work

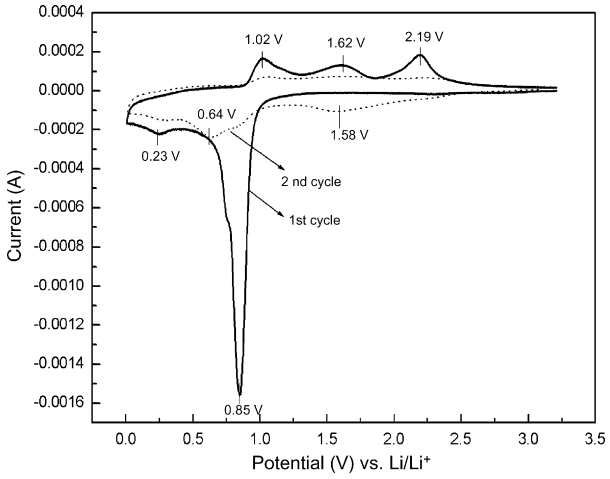

Fig. 5. Cyclic voltammograms of deposited film electrode of Co_3O_4 cycled between 0.01 and 3.0 V in 1 M $LiClO_4$ with PC electrolyte.

is different from that of Co_3O_4 bulk powder, but similar to that of Co_3O4 film electrode fabricated by PLD [13] where the discharge plateaus are at 0.91 and 0.6 V in the first discharge, and the subsequent discharge plateaus are at 0.9 and 1.4 V close to CoO bulk powder.

The discharge/charge curves of the Co_3O_4 electrodes in Li-ion test cell are shown in Fig. 6. During the first discharge, the potentials of the Co_3O_4 electrodes quickly falls to 1.0 V plateau and then gradually decline to the cut-off voltage of 0.01 V. The first discharge capacity about 1930 mAh g^{-1} was much more than 890 mAh g^{-1} the theoretical capacity of Co_3O_4. Although 730 mAh g^{-1} was lost, the left capacity of 1200 mAh g^{-1} after the second cycle was still more than the result of Poizot et al. [4], as shown in Fig. 7. Also, the capacity remained 500 mAh g^{-1} after the fiftieth cycle even at C/2. It is very promising for applications in lithium-ion batteries.

The much more capacity of the electrolytic Co_3O_4 coating was partly resulted from the larger effective surface and grain boundary area of nano-sized particles, as shown in Fig. 8(a), which may offer extra sites for Li ions. From cross-sectional

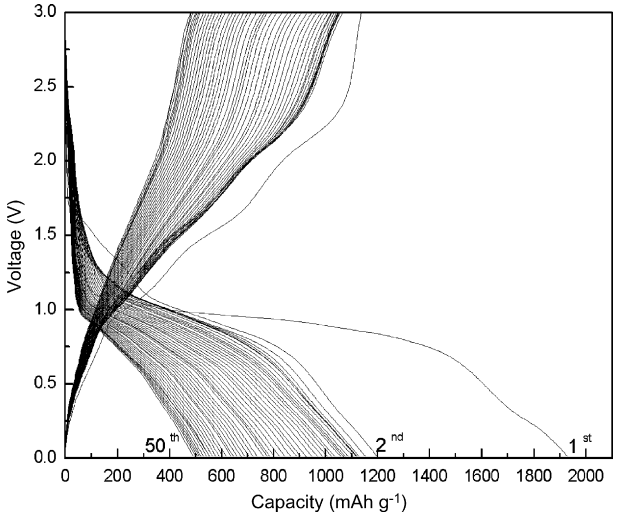

Fig. 6. Discharge-charge profiles on Li-ion test cell at 50 μA (C/2).

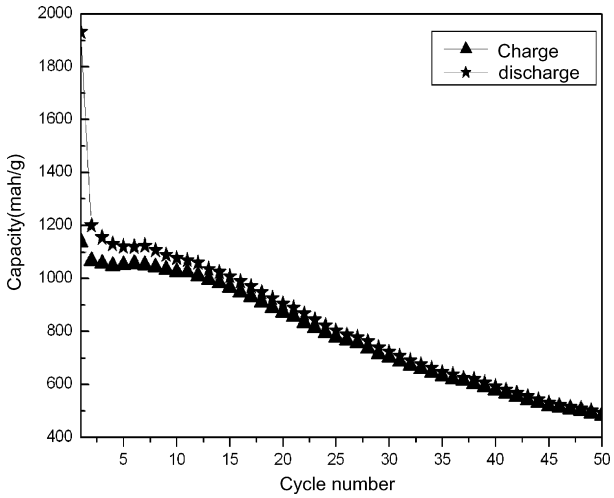

Fig. 7. Capacities of cobalt base oxides electrode versus cycle number.

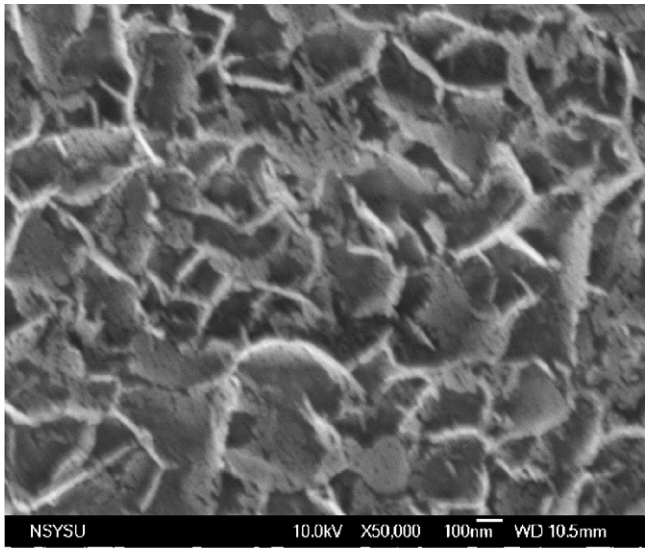

(a)

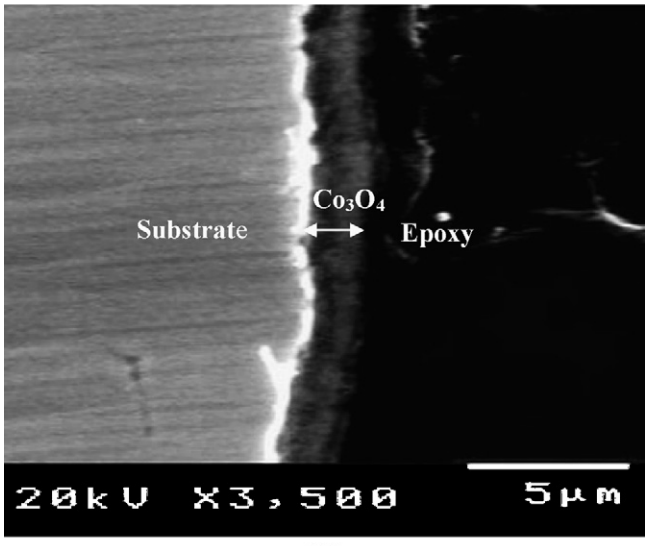

(b)

Fig. 8. The Co_3O_4 coated film (a) FE-SEM micrograph and (b) cross-sectional view after annealed at 400 °C for 5 h.

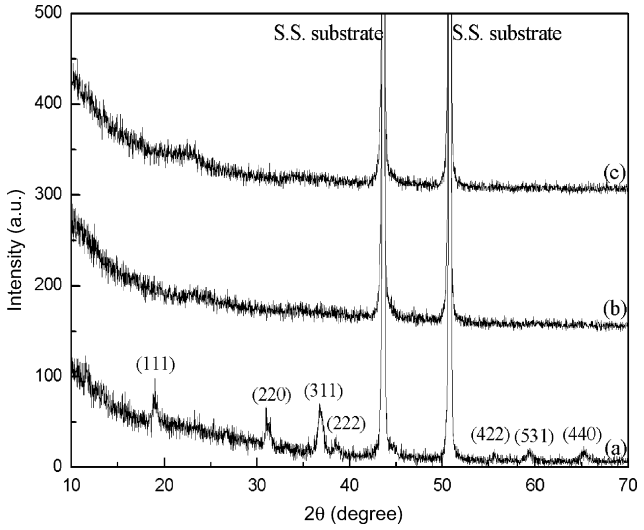

Fig. 9. Ex situ XRD patterns of (a) the Co_3O_4 coated specimen, (b) after a fully discharged to 0.01 V for 4 h, (c) a fully recharged to 3.0 V for 4 h.

view, the thickness was about 1.6 μm as shown in Fig. 8(b), and there was an adhesive interface between the coating and the substrate. However, some of the extra sites are irreversible for Li^+, resulting in the capacity loss in the first charging. To further examine the electrochemical processes of Co_3O_4 upon the first cycling, these lithiated and delithiated films were characterized by XRD and Raman spectra measurements. Ex situ X-ray diffractions have been conducted on Co_3O_4 electrodes in the fully lithiated and fully delithiated states which were sustained for 4 h, respectively. After fully lithiated state, the diffraction peaks of Co_3O_4 disappeared and only those of stainless steel remained, as shown in Fig. 9(a) and (b). The same results were found on the fully delithiated specimen, as shown in Fig. 9(c). Reasonably, the lithiated product should be Li_2O and Co, and the delithiated product CoO. However, Li_2O, Co and CoO have not been detected, because they were in the form of nano-sized particles. To further check these compounds, Raman spectra became another possible method to identify them. Raman spectrum of nano-sized Co_3O_4 revealed two strong peaks at 467 and 670 cm^{-1} accompanied broaden peak 512 cm^{-1} and sub-strong peaks at 482 and 692 cm^{-1} as shown in Fig. 10 diagram (b). The former two were not found before, and the later two were consistent with those of micro-sized Co_3O_4 [19]. Obviously, the nano-sized Co_3O_4 prepared by electrolytic deposition revealed its own characteristic of Raman spectra. After discharged to 0.1 V for 5 h the Co_3O_4 main peaks 482 and 692 cm^{-1} disappeared, at the same time the peak at 518 cm^{-1} were formed as shown in Fig. 10 diagram (c), which is close to 522 cm^{-1}, the standard peak of Li_2O, as shown in Fig. 10 diagram (a). It can be concluded that Li_2O phase was formed. Besides, two stronger peaks 477 and 681 cm^{-1} shifted toward the right about 10–11 cm^{-1} compared to those in Fig. 10 diagram (b), and another weaker peak 613 cm^{-1} were found. The type of these three peaks is similar to that of CoO but with increased wave number. When micro-sized particles become nano-sized, the increased surface and boundary area becomes a more and more important factor which gradually play a major factor on chemi-

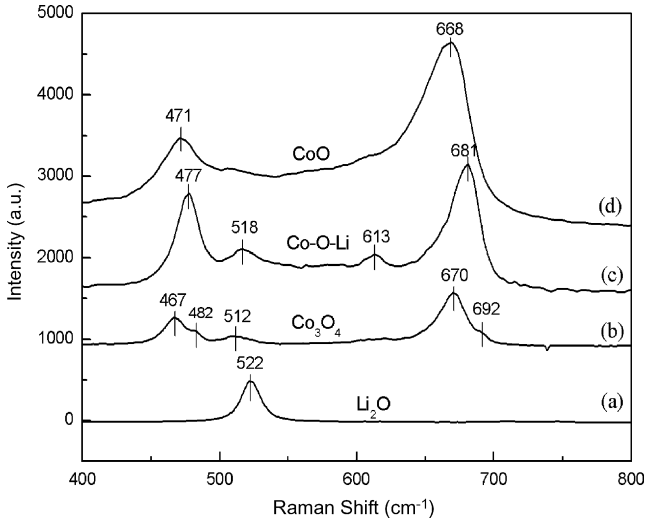

Fig. 10. Raman spectra of (a) Li_2O standard sample, (b) Co_3O_4 coated specimen annealed at 400 °C for 5 h, (c) discharged to 0.01 V for 4 h, and (d) recharged to 3.0 V for 4 h, during the first insertion-extraction process.

cal bonding, structure and hence the characteristics. Therefore, the interface between nano-sized Co metal particles and Li_2O matrix became one of the major chemical bonding. In other words, these three peaks (477, 681, and 613 cm^{-1}) may be the characteristics of Co-O-Li boding. After charged to 3.0 V for 5 h as shown in Fig. 10 diagram (d) the peak 518 cm^{-1} disappeared and 471 and 668 cm^{-1} appeared. The former one was resulted from the delithiation and the latter two from the formation of CoO. Compared with the main peaks 468 and 672 cm^{-1} of bulk CoO [20], they were shifted about 3–4 cm^{-1} because of the nano-sized effect. Obviously, Raman spectra are strongly affected by both particle size and interfacial bonding.

Based on the results of XRD and Raman spectra, the reduction and oxidation in the discharge/charge processes of Co_3O_4 are suggested as follows.

For the first cycle:
Discharge (lithiation):

$$Co_3O_4 + 8Li^+ + 8e^- \rightarrow 3Co + 4Li_2O \quad (10)$$

Charge (delithiation):(11)$Co + Li_2O \rightarrow CoO + 2Li^+ + e^-$
After the first cycle:

$$Co + Li_2O \rightleftarrows CoO + 2Li \quad (12)$$

Reaction (12) has been suggested [4]. Reaction (10) is an irreversible one of lithium ion in Co_3O_4 film, which produces nano-sized metallic cobalt and Li_2O. While charging, the metallic cobalt embedded in Li_2O matrix generates CoO instead of Co_3O_4 due to the similarity of oxygen lattices in Li_2O and β-CoO [21,13]. This irreversible reaction also played another important role on the dramatic loss of capacity during the first cycles, as shown in Figs. 6 and 7. In the subsequent steps, reaction (12) is reversible. It has been reported [22] that metal nanoparticle enhanced the formation/decomposition of Li_2O, in which nano-sized Co particles embedded, by favoring the Li_2O formation/decomposition reversible process rather than the electrolyte decomposition, with which they have no contact. As a result, the electrolytic Co_3O_4, finally CoO, still revealed the reversible capacity of 500 mAh g^{-1} even at C/2 after 50 cycles. It is noted that the present cycling decay is faster than that of CoO and Co_3O_4 reported by Poizot et al. [4] and Wang et al. [13], close to nanorods and nanoparticle by Li et al. [8], however better than that of HT-Co_3O_4, LT-Co_3O_4, ball-milled Co_3O_4 and CoO by Wang et al. [6]. This means that both of morphology and particle size have the influence on the electrode cycle life.

4. Conclusions

Electrolytic deposition method has been successfully used to fabricate Co_3O_4 thin film electrodes for Li batteries. The as-coated film was composed of β-$Co(OH)_2 \cdot H_2O$, condensed into CoO and further oxidized into naon-sized Co_3O_4 particles, after annealed at 400 °C for 5 h. Through FE-SEM observations, Raman spectra analysis, XRD and discharging/charging tests, the nano-sized Co_3O_4, CoO, Co and Li_2O particles revealed their own characteristics different from micro-sized particles, such as more interfacial effects on chemical bondings and crystallinity. Its capacity much more than theoretical value may be resulted from the more interfacial bondings of nano-sized particles which offering extra sites for Li^+ insertion. The dramatically irreversible capacity of the first discharging was caused by the irreversible reaction of Co_3O_4 in reaction (10) and the irreversible trapping of Li^+ in extra sites. After the first cycle, the subsequent steps were reversible reactions involving the oxidation and reduction between nano-sized Co and CoO in reaction (12). Still, it offered the reversible capacity as high as 500 mAh g^{-1} at C/2 after 50 cycles.

Acknowledgments

The authors are grateful for the support of this research by the National Science Council, Republic of China under contract No. NSC 94-2622-E-005-014-CC3.

References

[1] I.A. Courtney, J.R. Dahn, J. Electrochem. Soc. 144 (1997) 2045–2052.
[2] G.R. Goward, F. Leroux, W.P. Power, G. Ouvrard, W. Dmowski, T. Egami, L.F. Nazar, Electrochem. Solid-State Lett. 2 (1999) 367–370.
[3] J. Morales, L. Sanchez, J. Electrochem. Soc. 146 (1999) 1640–1642.
[4] P. Poizot, S. Laruelle, S. Grugeon, L. Dupont, J.-M. Tarascon, Nature 407 (2000) 496–499.
[5] F. Badway, I. Plitz, S. Grugeon, S. Laruelle, M. Dolle', A.S. Gozdz, J.M. Tarascon, Electrochem. Solid State Lett. 5 (2002) A115–A118.
[6] G.X. Wang, Y. Chen, K. Konstantinov, M. Lindsay, H.K. Liu, S.X. Dou, J. Power Source 109 (2002) 142–147.
[7] D. Larcher, G. Sudant, J.-B. Leriche, Y. Chabre, J.-M. Tarascon, J. Electrochem. Soc. 149 (2002) A234–A241.
[8] W.Y. Li, L.N. Xu, J. Chen, Adv. Funct. Mater. 15 (2005) 851–857.
[9] T. Seike, J. Nagai, Sol. Energy Mater. 22 (1991) 107–117.
[10] C.N. Polo da Fonseca, M.A. de Paoli, A. Gorenstein, Adv. Mater. 3 (1991) 553–555.
[11] T. Maruyama, S. Arai, J. Electrochem. Soc. 143 (1996) 1383–1386.
[12] F. Svegl, B. Orel, I.G. Svegl, V. Kaucic, Electrochim. Acta 45 (2000) 4359–4371.

[13] Z.W. Fu, Y. Wang, Y. Zhang, Q.Z. Qin, Solid State Ionics 170 (2004) 105–109.
[14] F.A. Cotton, C. Wilkinson, Advanced Inorganic Chemistry-A Comprehensive Test, fourth ed., John Wiley & Sons, Inc, New York, 1980.
[15] M. Pourbaix, Atlas of Electrochemical Equilibria in aqueous Solutions, NACE, Houston, TX, 1974, p. 325.
[16] C. Liu, J.A. Ritter, B.N. Popov, J. Electrochem. Soc. 145 (12) (1998) 4097–4103.
[17] Z.P. Xu, H.C. Zeng, J. Mater. Chem. 8 (1998) 2499–2506.
[18] M. Oku, Y. Sato, Appl. Surf. Sci. 55 (1992) 37–41.
[19] V.G. Hadjiev, M.N. Iliev, I.V. Vergilov, J. Phys. C: Solid State Phys. 21 (1988) L199–L210.
[20] H.C. Choi, Y.M. Jung, I. Noda, S.B. Kim, J. Phys. Chem. B 107 (2003) 5806–5811.
[21] M.N. Obrovac, R.A. Dunlap, R.J. Sanderson, J.R. Dahn, J. Electrochem. Soc. 148 (2001) A576–A588.
[22] P. Poizot, S. Laruelle, S. Grugeon, L. Dupont, J.M. Tarascon, J. Power Sources 97–98 (2001) 235–239.